# Surface and subsurface dynamics of a perennial slow-moving landslide from ground, air and space

Xie Hu[1*], Roland Bürgmann[1], William H. Schulz[2], and Eric J. Fielding[3]

[1] Department of Earth and Planetary Science, University of California, Berkeley, California, USA

[2] U.S. Geological Survey, Denver, CO, USA

[3] Jet Propulsion Laboratory, California Institute of Technology, Pasadena, CA, USA

Correspondence to: xiehu@berkeley.edu

This is a non-peer reviewed pre-print submitted to EarthArXiv. This paper has been submitted to *Nature Communication* for review.

**Landslides modify the natural landscape and cause fatalities and property damage worldwide. Quantifying landslide dynamics is challenging due to the stochastic nature of the environment. With its large area of ~1 km$^2$ and perennial motions at ~10-20 mm/day, the Slumgullion landslide in Colorado, USA represents an ideal natural laboratory to better understand landslide behavior. Here we use hybrid remote sensing data and methods to recover the four-dimensional surface motions during 2011-2018. We resolve a new mobile area of ~0.35 km$^2$ below the crest of the prehistoric landslide. We construct a mechanical framework to quantify the rheology, subsurface channel geometry, mass flow rate, and spatiotemporally dependent pore-water pressure feedback through a joint analysis of displacement and hydrometeorological measurements from ground, air and space. Variations in recharge, mainly from snowmelt, drive multi-annual decelerations and accelerations, during which the head of the landslide is the most responsive. Our study demonstrates the importance of remotely characterizing often inaccessible, dangerous slopes to better understand landslide mechanisms, landscape modification, and other quasi-static mass fluxes in natural and industrial environments, and will ultimately help reduce landslide hazards.**

Landslides denude mountains, transport sediments to rivers, lakes and oceans, and modify the Earth's surface environment and ecosystem. Landslides of all sizes and rates represent geohazards that may lead to property damage and casualties. The hazards that landslides present and their impact on Earth's surface primarily depend on their volume and the rate at which they move, as well as their responsiveness to hydroclimatic variability. However, quantifying landslide dynamics is challenging due to the stochastic nature of the environment (e.g., geology, geomorphology, vegetation), external disturbances (e.g., fire, climate change, earthquakes, logging), and the limited availability of observations (e.g., remote, surface and subsurface geodetic, geophysical and hydrological measurements)[1-5]. Knowledge of landslide behavior primarily depends on isolated measurements made on and within the landslides, which are often cost prohibitive or even impossible to obtain, and their value is limited by conservative interpretations for generalizing to the entirety of dynamically complex landslides. Incomplete information of three-dimensional (3D) surface displacements has limited our ability to infer the continuous landslide depth, interpret the driving and resisting mechanisms, and develop accurate forecasts for landslides. Here we compile a comprehensive dataset of remote sensing imagery from air and space, meteorological records, and in-situ surface (extensometer) and subsurface (inclinometer) deformation measurements, allowing us to develop a systematic framework for using detailed, temporally-variable 3D surface deformation data to quantify the underlying landslide kinematics and dynamics.

For centuries, the Slumgullion landslide in the San Juan Mountains of Colorado has snaked its way downhill at ~10-20 mm/day[5-16], allowing us to explore both transient and quasi steady-state mass wasting processes. The original 700-year-old failure initiated from the edge of the Cannibal Plateau, formed Lake San Cristobal, and is currently inactive (Fig. 1). About 300 years ago, an

approximately 3,900-m-long and 150- to 450-m-wide section of the landslide reactivated from the original headscarp to a new toe above Highway 149. The landslide deposits consist of hydrothermally altered Tertiary volcanic rocks.

Interferometric Synthetic Aperture Radar (InSAR) has been widely used to measure ground motions for geohazards research[17-19], but its application at Slumgullion is challenged by high deformation gradients. Additionally, the reconstruction of 3D surface displacements depends on the availability of multiple view angles and their distribution[16, 20]. Here we incorporate data from the ascending and descending tracks of Copernicus spaceborne C-band Sentinel-1 SAR (2017-2018) and four flight lines of the NASA/JPL airborne L-band Uninhabited Aerial Vehicle SAR (UAVSAR) (2011-2018; Fig. 1A) with a hybrid InSAR phase and SAR amplitude pixel offset tracking (POT) time-series analysis (Figs. S1-S2; Table S1)[21-22]. The advance in data and method integration illuminates the spatiotemporal 3D surface evolution from 1000+ individual displacement maps (Figs. S3-S4), two orders of magnitude more than previous SAR-based studies[14-16].

## Results

### Spatial displacement patterns

The 98-scenes of Sentinel-1 SAR reveal displacement details over the more slowly deforming head and toe areas of the landslide (Fig. 1B-C). The fast-moving middle parts are not resolvable due to extreme InSAR phase gradients at the available Sentinel-1 orbital period, radar wavelength, and the amount of displacement over a short distance (see Methods). We recognize a new kinematic element in an area of ~0.35 $km^2$ below the crest of the prehistoric landslide (Fig. 1A), which

accounts for ~1/3rd of the previously mapped mobile area[8-9, 14]. We further update the structural zones[9]: head zone (kinematic elements #1-3) exposed by extensional fractures, zone of stretching (#4-6) characterized by broad bands of tension cracks and normal faults, hopper & neck (#7-8) resembling a funnel, zone of marginal pull-apart basins (#9-10) accompanying widening of the slide, and toe (#11-12) overriding inactive surfaces. The current major source of debris supply appears to be on the upper flank of the head (blackish area in Fig. 1B-C with motion to east). Here, the sediments are transported along a curved track parallel to the margin between elements 1 and 2, at a large angle from the main stream of the slide.

To systematically analyze the kinematics and mechanics of Slumgullion, we rely on 3D velocity fields that describe the steady state, slow-moving earth flow. We obtain eight velocity measurements from four UAVSAR flight lines during each sortie in their respective azimuth and range directions. The hybrid InSAR-POT analysis provides us a robust 3D solution over the entire active landslide area, with a total of 124 scenes. We represent the deformation in a series of 77 transverse profiles (Figs. 2A and S5). The displacements in the steep upper head zone are highly variable with low signal-to-noise ratio (SNR). Velocity measurements become more coherent from the intersection between the head and the zone of stretching, moving at about 2.5 mm/day. The south part of the zone of stretching moves at 7 mm/day, and elongated flank ridges extend along its southeastern lateral margin (Fig. S5). The movement rotates westerly to the narrow hopper & neck. The velocity profiles regain a symmetric pattern with rates as high as 13 mm/day at the center. The surface topography gradually develops a bump along the central axis (Fig. S5). The rates decrease to ≤10 mm/day in the zone of marginal pull-apart basins, and the velocity profiles appear asymmetric around the internal bends. An oversteepened northwest-facing slope divides

the toe, and the southern part moves faster along this internal right-lateral fault at up to 6 mm/day. The persistently advancing landslide toe results in shifted fronts with respect to those mapped in the summer of 1991[8]. Multiple pieces of evidence validate the advance of the toe over its substrate. UAVSAR-derived 2011-2018 horizontal velocities at the tip of the toe reach 4-5 mm/day, consistent with the rate determined from aerial photos taken in 1985 and 1990 (ref. *9*). The mapped shifts (Fig. 3) and the topographic back-projection (Fig. S6) also show that the toe has advanced by ~40 m during the past two decades.

**Inferred landslide channels and subsurface flow**

The transverse longitudinal velocities allow us to invoke the depth-integrated law of mass conservation in order to estimate the local free-surface height from the slide channel bottom. Viscoplastic flow models suggest that the longitudinal shear velocities at the surface mirror the shape of the subsurface channel[23, 24]. We propose a novel geometric description of the landslide channel, which characterizes the depth, the steepness between the basal bed surface and the lateral margins, and the tilt of the basal bed across the landslide with respect to the horizontal (Figs. 2 and S7-S10). We use the longitudinal surface-velocity profiles to invert for these geometric parameters. The largest depth (<~30 m) is inferred underneath the fastest-moving hopper & neck. High steepness values concentrate at the zone of marginal pull-apart basins in the lower part of the slide. According to the inferred degree of bed tilting, the head and toe areas are more asymmetric, consistent with their irregular outlines. The bed starts from a minor NW tilt in the zone of stretching and transitions to the largest positive SE tilt at the biggest bend of the slide. Our quantification of the landslide geometry yields a total volume of $1.33\times10^7$ $m^3$, compared to a previous estimate of $1.95\times10^7$ $m^3$ (ref. *8*).

We can also resolve the subsurface viscoplastic flow rate along with the channel geometry (Fig. 2C-E). Insignificant shear deformation down to about 10-m depth found at the borehole inclinometer indicates that the landslide materials are highly plastic and follow non-Newtonian behavior (Fig. S11). Additionally, SAR and extensometer measurements at lateral flanks reveal appreciable highly localized deformation that suggests a pseudo-plastic rheology at shallow depths. Therefore, we apply the power-law flow theory to characterize the upper pseudo-plug and the lower yield zone above the underlying bedrock[25] (see Methods). We can quantify the power-law index as 0.7 and the consistency index as $1.34\times10_{10}$ $Pa\cdot s^n$ based on the inferred landslide thickness at the distal toe (Fig. S12; Table S2). High velocity gradients concentrate near the bottom of the slide and approach 0 at shallower depths (Fig. 2C).

**Hydrological forcing and time-dependent landslide deformation**

We also explore the landslide behavior controlled by the time-variant hydrological environment. As fluid water is the essential agent that regulates the pore pressure[1, 26-27], we explicitly consider the forms of precipitation and determine the daily fluid water from snowmelt and rainwater (see Methods). The water year 2018 (10/1/2017-9/30/2018) was historically dry with only 64% of 1981-2010 precipitation average. There was another dry water year in 2013 from the estimated fluid water recharge, however this is barely discernible from raw precipitation data (Fig. 4B and Fig. S13). From the recharge time series we simulate pore pressures at depth as a one-dimensional diffusive process from the surface (see Methods; Fig. S14).

We investigate the slide's temporal response to the estimated seasonal and multi-annual fluid water changes by comparing Sentinel-1 InSAR results of August in 2017 (wet) and 2018 (dry), for which time-series solutions are available for both tracks (Fig. 4A). Between the two time periods, radar line-of-sight (LOS) rates slowed down by 90% at high elevations (3450 m), the rate reduction decreases linearly to 70% over the upper slide (3300 m elevation), while it is only around 45% in the toe area (2950-3100 m elevation). Extensometers located on the southern flanks of elements 6, 10 and 12 show decelerations by 66%, 40% and 49%, respectively, between the same periods (Fig. 3B). The variable rate decreases in response to the reduced water recharge imply spatiotemporal diversity of pore pressure feedback.

The UAVSAR hybrid InSAR and POT analysis captures the temporal behavior of the whole landslide during 2011-2018 at a coarser temporal sampling (Fig. 4B; Figs. S15-S16). The time series of downslope motions from UAVSAR and three extensometers match well (Fig. 3B). Based on the long-term changes in the fluid-water recharge history, we consider three multi-annual phases of 08/2011-11/2013, 04/2013-11/2017, and 10/2016-10/2018. We use an exponential model to quantify the multi-annual rate changes (i.e., the velocity changes with respect to initial conditions for each period, see Methods). Element 1 was excluded due to small SNR. Agreeing well with the hydrological processes, the inferred rate changes are negative for 2011-2013 and 2016-2018, indicative of slowing down, contrasting with the inferred speeding up during 2013-2017 (Figs. 4 and S17-S18). The head area consistently responds most sensitively to recharge changes during all three phases (Fig. 4C).

The distribution of UAVSAR-measured rate changes with position on the landslide is consistent with the deceleration vs. elevation/position relationship observed during 2017-2018 with Sentinel-1, as well as the extensometer data. This suggests a correlation between the landslide depth and sensitivity to hydrological forcing. This is physically consistent because the diffusive pore pressure changes more strongly and rapidly at shallow depths, while the response is increasingly damped and delayed at greater depths. For example, the onset of the pore-pressure increase at 20-m depth lags behind that at 10-m depth by ~12 days according to the constrained diffusion model adjusted by the average pore pressure measured previously[12] of 177 kPa (Fig. S14).

**Implications for the perennial motions of landslides**

Water recharge at the Slumgullion increases twice per year, from snowmelt in late spring and rainfall in early fall, which results in a more stable nearly saturated system than landslides that experience only one significant annual recharge episode. For instance, the near-saturation condition can last for about half time of the year from March at a characteristic depth of 20 m (Fig. S14). Our results also show that over time scales of several years, the Slumgullion accelerates and decelerates due to multi-year hydrological fluctuations, supporting the hypothesis that it and other landslides in the Rocky Mountains will slow in future decades due to predicted temperature increases, precipitation decreases, and a depletion of supply[13]. Other factors, such as changes in vegetation cover and possible large failures at the headscarp, could make the situation more complicated[13]. Moreover, other stabilizing mechanisms, such as shear strength that increases with shear displacement rate, shear-induced dilative strengthening, soil wetting and swelling along the lateral margins above the water table, and the forced circulation of pore fluid around asperities may help augment the resistance[27-30]. Hourly sampled subsurface strain and pore pressure data and

laboratory testing may be able to identify and distinguish these contributions to the landslide strength. If such forces play a role, we can qualitatively determine that the landslide neck with large contact areas along the sides, and the zones of hopper & neck and pull-apart basins that have large irregularities in landslide depth and steepness, may provide additional stabilizing force.

Unprecedented, interdisciplinary observations, methods and models combined help to advance the characterization of landslide dynamics. Remotely sensed SAR data and hybrid processing methods allow us to achieve 3D spatiotemporal surface displacements. In-situ datasets such as the extensometer measurements validate and calibrate the SAR results from air and space; the inclinometer data provide evidence on the non-Newtonian behavior of the landslide mass, together with the SAR/extensometer-confirmed mobility at the margins, support the application of power-law viscoplastic flow theory; the precipitation and temperature records illuminate the fluid recharge from snowmelt and rainwater; the piezometer-measured average pore pressures help translate recharge at the surface to pore pressures at depth. Our study sheds new light on the landslide boundaries, geometry, subsurface flow, and how different structural zones respond to the hydroclimatic variability. Beyond that, our systematic chains of analysis can also be applied in full or in part to help understand other quasi-static viscoplastic flow processes associated with solid particles with an interstitial fluid, such as debris slides, volcanic lahars, and submarine slides.

**References:**


1. Iverson, R. M. & LaHusen, R. G. Dynamic pore-pressure fluctuations in rapidly shearing granular materials. *Science* **246**, 796–799 (1989).
2. Schulz, W. H., Kean, J. W. & Wang, G. Landslide movement in Southwest Colorado triggered by atmospheric tides. *Nat. Geosci.* **2**, 863–866 (2009).
3. Roering, J. J., Mackey, B. H., Handwerger, A. L., Booth, A. M., Schmidt, D. A., Bennett, G. L. & Cerovski-Darriau, C. Beyond the angle of repose: A review and synthesis of landslide processes in response to rapid uplift, Eel River, Northern California. *Geomorphology* **236**, 109–131 (2015).
4. Kargel, J. S., et al. Geomorphic and geologic controls of geohazards induced by Nepal's 2015 Gorkha earthquake. *Science* **351**, aac8353 (2016).
5. Palmer, J. Creeping earth could hold secret to deadly landslides. *Nature* **548**, 384–386 (2017).
6. Howe, E. Landslides in the San Juan Mountains, Colorado. *US Geol. Surv. Professional Paper* 67 (US Geological Survey, 1909).
7. Crandell, D. R. & Varnes, D. J. Movement of the Slumgullion earthflow near Lake City, Colorado. *US Geol. Surv. Professional Paper* 424-B (US Geological Survey, 1961).
8. Parise, M. & Guzzi, R. Volume and shape of the active and inactive parts of the Slumgullion landslide, Hinsdale County, Colorado. *US Geol. Surv. Open-File Report* 92-216 (US Geological Survey, 1992).
9. Fleming, R. W., Baum, R. L. & Giardino, M. Map and description of the active part of the Slumgullion landslide, Hinsdale County, Colorado. *US Geol. Surv. Geol. Inv. Ser. Map* I-2672 (U.S. Geological Survey, 1999).

10. Coe, J. A., Ellis, W. L., Godt, J. W., Savage, W. Z., Savage, J. E., Michael, J. A., et al. Seasonal movement of the Slumgullion landslide determined from Global Positioning System surveys and field instrumentation, July 1998–March 2002. *Eng. Geol.* **68**, 67–101 (2003).
11. Coe, J. A., Mckenna, J. P., Godt, J. W. & Baum, R. L. Basal-topographic control of stationary ponds on a continuously moving landslide. *Earth Surf. Proc. Land.* **34**, 264–279 (2009).
12. Schulz, W. H., Mckenna, J. P., Kibler, J. D. & Biavati, G. Relations between hydrology and velocity of a continuously moving landslide—Evidence of pore-pressure feedback regulating landslide motion? *Landslides* **6**, 181–190 (2009).
13. Coe, J. A. Regional moisture balance control of landslide motion: Implications for landslide forecasting in a changing climate. *Geology* **40**, 323–326 (2012).
14. Schulz, W. H., Coe, J. A., Ricci, P. P., Smoczyk, G. M., Shurtleff, B. L. & Panosky, J. Landslide kinematics and their potential controls from hourly to decadal timescales: Insights from integrating ground-based InSAR measurements with structural maps and long-term monitoring data. *Geomorphology* **285**, 121-136 (2017).
15. Milillo, P., Fielding, E. J., Schulz, W. H., Delbridge, B. G. & Bürgmann, R. COSMO-SkyMed spotlight interferometry over rural areas: The Slumgullion landslide in Colorado, USA. *IEEE J. Sel. Topics Appl. Earth Observ. Remote Sens.* **7**, 2919–2926 (2014).
16. Delbridge, B. G., Bürgmann, R., Fielding, E. J., Hensley, S. & Schulz, W. H. 3D surface deformation derived from airborne interferometric UAVSAR: Application to the Slumgullion landslide. *J. Geophys. Res.* **121**, 3951–3977 (2016).

17. Bürgmann, R., Rosen, P. A. & Fielding, E. J. Synthetic aperture radar interferometry to measure Earth's surface topography and its deformation. *Annual Rev. Earth Planet. Sci.* **28**, 169–209 (2000).

18. Hilley, G. E., Bürgmann, R., Ferretti, A., Novali, F. & Rocca, F. Dynamics of slow-moving landslides from permanent scatterer analysis. *Science* **304**, 1952–1955 (2004).

19. Hu, X., Lu, Z., Pierson, T. C., Kramer, R. & George, D. L. Combining InSAR and GPS to determine transient movement and thickness of a seasonally active low-gradient translational landslide. *Geophysical Res. Lett.* **45**, 1453–1462 (2018).

20. Hu, X., Bürgmann, R., Lu, Z., Handwerger, A. L., Wang, T. & Miao, R. Mobility, thickness, and hydraulic diffusivity of the slow-moving Monroe landslide in California revealed by L-band satellite radar interferometry. *J. Geophys. Res.* **124** (2019).

21. Hensley, S., Wheeler, K., Sadowy, G., Miller, T., Shaffer, S., Muellerschoen, R., Jones, C., Zebker, H., Madsen, S. & Rosen, P. Status of a UAVSAR designed for repeat pass interferometry for deformation measurements. *IEEE MTT-S International Microwave Symposium* **3**, 1453-1456 (2005).

22. Hu, X., Wang, T. & Liao, M. Measuring coseismic displacements with point-like targets offset tracking. *IEEE Geosci. Remote Sens. Lett.* **11**, 283-287 (2014).

23. Mei, C. C. & Yuhi, M. Slow flow of a Bingham fluid in a shallow channel of finite width. *J. Fluid Mech.* **431**, 135–159 (2001).

24. van Asch, T. W. J., Van Beek, L. P. H. & Bogaard, T. A. Problems in predicting the mobility of slow-moving landslides. *Eng. Geol.* **91**, 46-55 (2007).

25. Longo, S., Di Federico, V. & Chiapponi, L. Propagation of viscous gravity currents inside confining boundaries: the effects of fluid rheology and channel geometry. *Proc. R. Soc. A* **471** (2015).

26. Cohen-Waeber, J., Bürgmann, R., Chaussard, E., Giannico, C. & Ferretti, A. Spatiotemporal patterns of precipitation-modulated landslide deformation from independent component analysis of InSAR time series. *Geophys. Res. Lett.* **45** (2018).

27. Handwerger, A. L., Fielding, E. J., Huang, M.-H., Bennett, G. L., Liang, C. & Schulz, W. H. Widespread initiation, reactivation, and acceleration of landslides in the northern California Coast Ranges due to extreme rainfall. *J. Geophys. Res.* **124**, 1782–1797 (2019).

28. Iverson, R. M., Reid, M. E., Iverson, N. R., LaHusen, R. G., Logan, M., Mann, J. E. & Brien, D. L. Acute sensitivity of landslide rates to initial soil porosity. *Science* **290**, 513–516 (2000).

29. Schulz, W. H., Smith, J. B., Wang, G., Jiang, Y. & Roering, J. J. Clayey landslide initiation and acceleration strongly modulated by soil swelling. *Geophys. Res. Lett.* **45**, 1888–1896 (2018).

30. Baum, R. L. & Johnson, A. M. Steady movement of landslides in fine-grained soils: A model for sliding over an irregular slip surface. *US Geol. Surv. Bull.* 1842 (US Geological Survey, 1993)

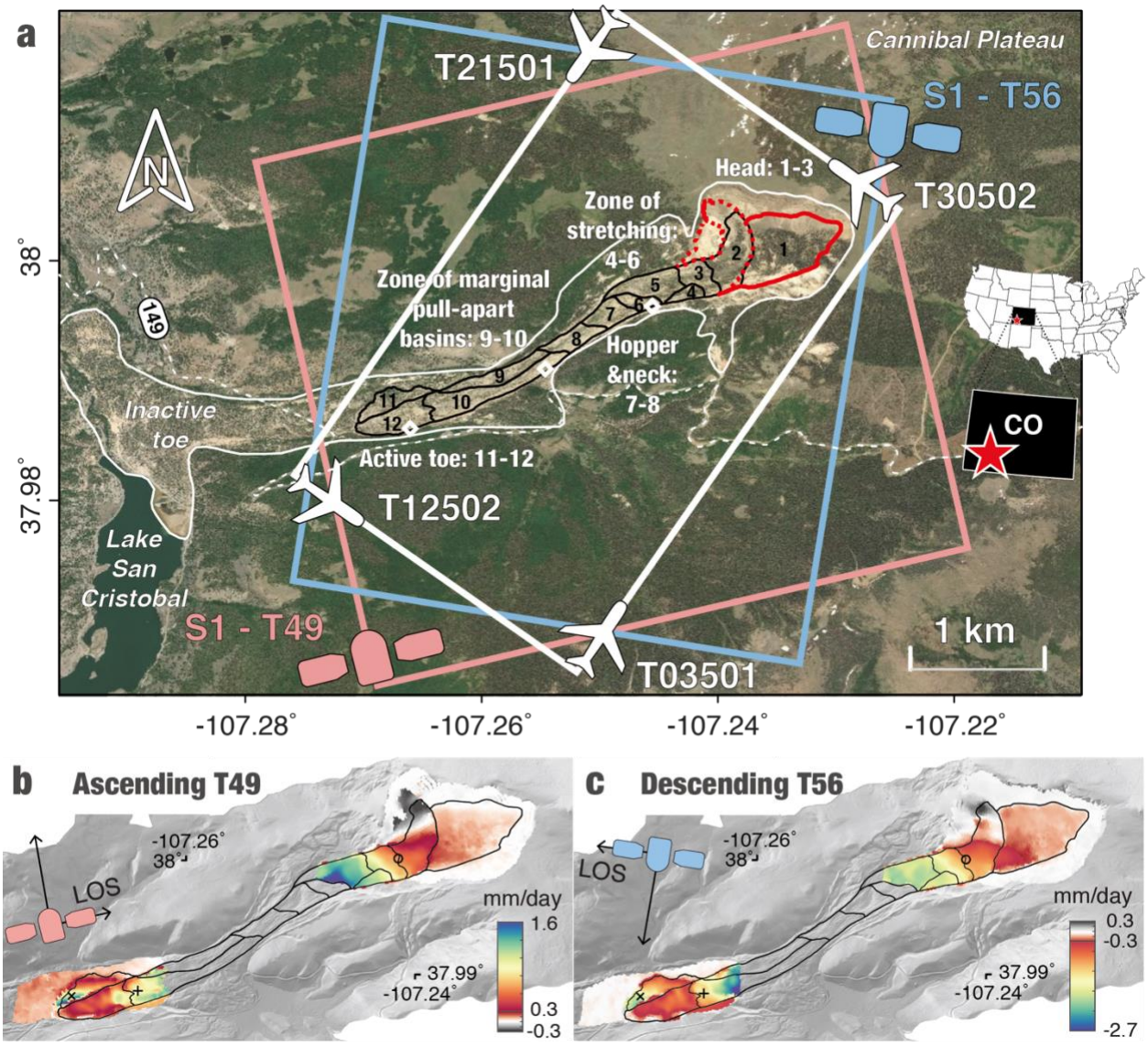


**Figure 1. Map of the Slumgullion landslide. a**, Landslide landscape. Red and blue boxes show swaths from Sentinel-1 ascending (T49) and descending (T56) tracks, respectively. White box shows UAVSAR swaths. Black and gray lines outline the active and inactive landslides. White diamonds show the locations of three extensometers. Structural zones and kinematic elements are labeled[8-9, 14]. Red lines show updated boundaries from this study, and dashed lines are tentative. **b&c,** Sentinel-1 line-of-sight (LOS) displacements positive towards the satellite,

superimposed on the shaded relief LiDAR DEM. Three symbols (o\x\+) show targets with time-series plots in Fig. 4a.

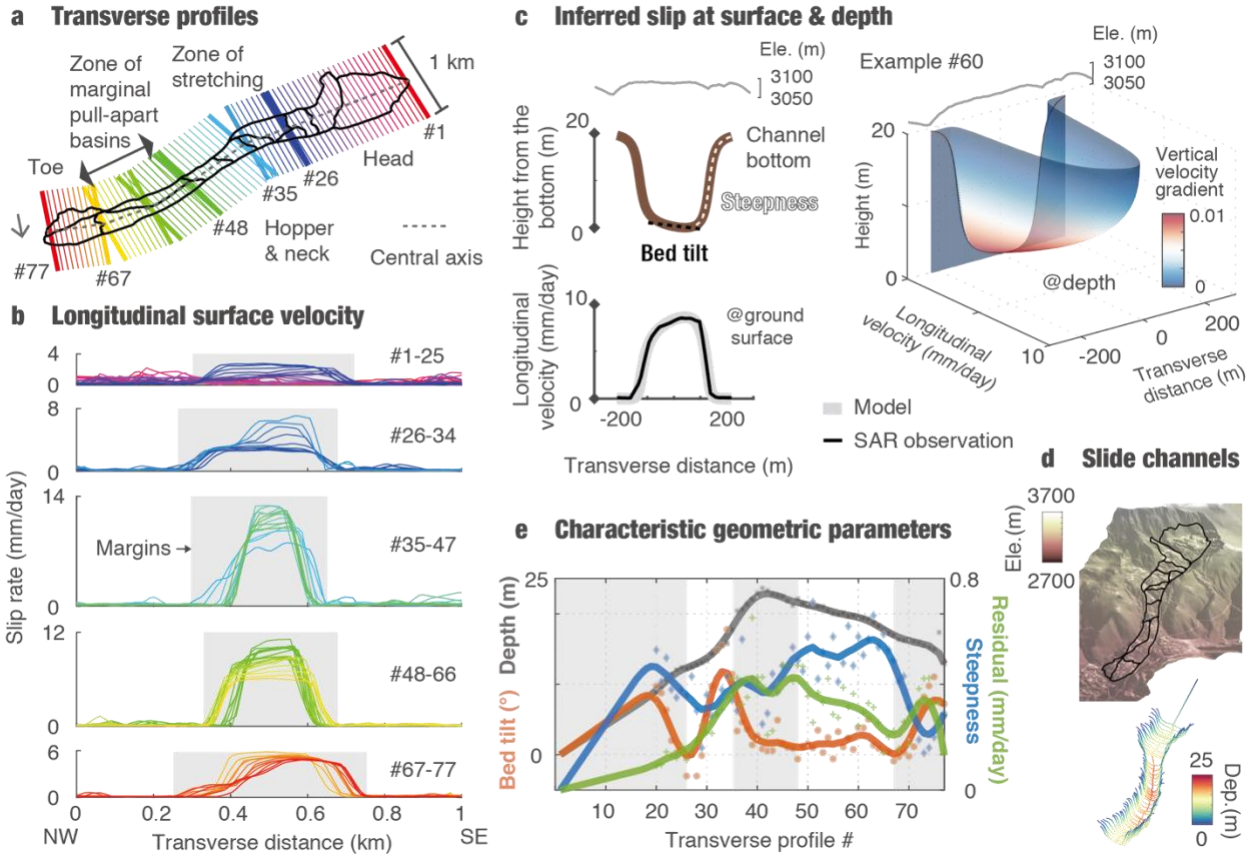


**Figure 2. Surface and subsurface landslide kinematics. a**, Transverse profiles selected every 50 m and differentiated by colors; the dashed gray line delineates the central axis. **b**, Longitudinal surface velocity from hybrid InSAR/POT analysis of UAVSAR data; colored lines represent 1-km-long profiles in **a**; shaded sections are within the lateral margins determined by the velocity profiles. **c**, Example of the inferred channel geometry and slip rates at the surface (compared with SAR results) and subsurface. Geometric steepness and bed tilt are indicated by white and black dashed lines, respectively. **d**, 3D view of landslide surface and the inferred basal morphology. **e**, Changing characteristic geometric parameters along the landslide. Symbols are the individual results for each profile with fitting lines in corresponding colors also used for y-axis labels.

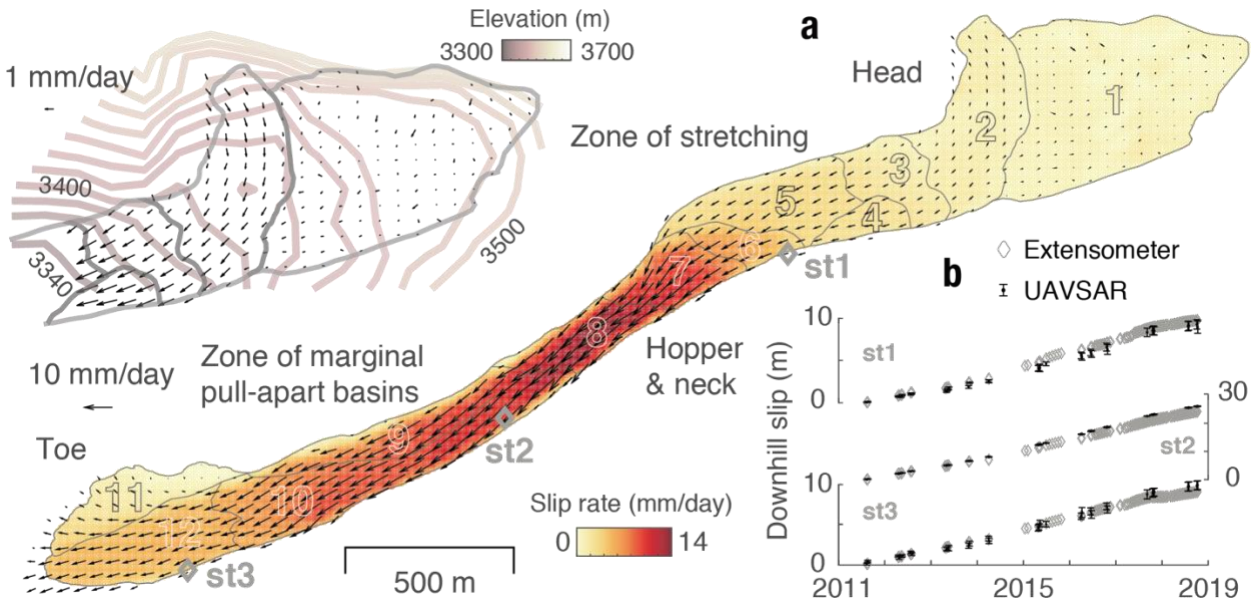


**Figure 3. Landslide spatial dynamics. a**, Horizontal slip vectors derived from 2011-2018 UAVSAR data with net 3D velocities in color. Inset close-up view of the head also shows elevation contours. **b**, Comparisons between UAVSAR time series and data from three extensometers (locations as in **a**).

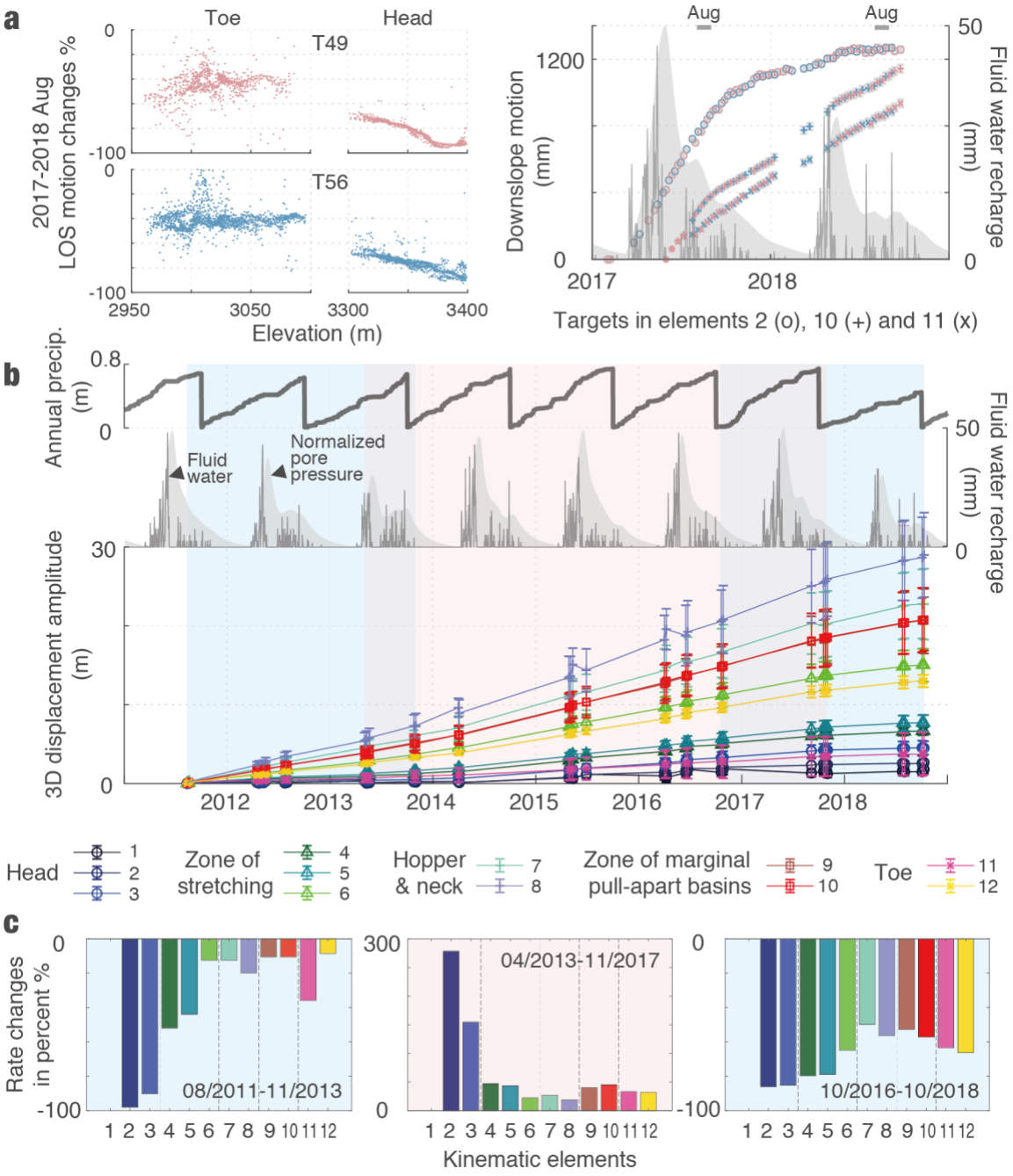


**Figure 4. Multi-annual landslide motions. a**, Results from Sentinel-1 ascending (red) and descending (blue) data. The left panel shows the line-of-sight velocity changes between August 2017 and 2018 over the head and toe, plotted against the elevation. The right panel shows the downslope motion of selected targets (locations in Fig. 1). **b**, 3D displacement amplitude for each kinematic element in indicated colors from UAVSAR hybrid InSAR-POT analysis. Blue and red

shades on the background show the time periods of observed deceleration and acceleration, respectively, consistent with the meteorological data. The annual precipitation observations, the estimated water recharge at the surface, and the normalized pore pressure at 20-m depth are shown in gray thick, thin lines and shades, respectively. **c**, Multi-year rate changes in three respective periods for the kinematic elements.

**Acknowledgments:**

We thank the UAVSAR flight and data processing teams for acquiring the data and processing the SLC stacks. We thank all the data providers – UAVSAR, Sentinel-1, LiDAR DEM, meteorological data can be freely downloaded from the NASA/JPL, Copernicus Open Access Hub and Alaska Satellite Facility, OpenTopography, and U.S. Natural Resources Conservation Service, respectively. This research was sponsored by the NASA Earth Surface and Interior Geodetic Imaging program. Part of this research was performed at the Jet Propulsion Laboratory, California Institute of Technology under contract with NASA. Mention of trade names or commercial products is not an endorsement or recommendation for use by the U.S. Government.